Supplementary Information for: Chemical and isotopic composition of secondary organic aerosol generated by α-pinene ozonolysis

Carl Meusinger[1], Ulrike Dusek[2,3], Stephanie M. King[1,4], Rupert Holzinger[2], Thomas Rosenørn[1,5], Peter Sperlich[6,7], Maxime Julien[8], Gerald S. Remaud[8], Merete Bilde[1,9], Thomas Röckmann[2], and Matthew S. Johnson[1]

[1]Department of Chemistry, University of Copenhagen, DK 2100, Copenhagen Ø, Denmark
[2]Institute for Marine and Atmospheric research Utrecht (IMAU), Utrecht University, 3584 CC, Utrecht, The Netherlands
[3]Centre for Isotope Research, Energy and Sustainability Research Institute Groningen, 9747 AG Groningen, The Netherlands
[4]now at: Haldor Topsøe A/S, DK 2800, Kgs. Lyngby, Denmark
[5]Infuser ApS, DK 2200, Copenhagen N, Denmark
[6]Max-Planck Institute for Biogeochemistry, 07745 Jena, Germany
[7]now at: National Institute of Water and Atmospheric Research (NIWA), Wellington 6021, New Zealand
[8]CEISAM, UMR CNRS6230, BP 92208, Nantes 44322 cedex 3, France
[9]now at: Aarhus University, Department of Chemistry, 8000 Aarhus C, Denmark

Correspondence to: C.M. (c.meusinger@gmail.com)

S1 Chamber setup

The design and operation mode of the aerosol chamber used in the α-pinene ozonolysis experiments (as shown in Fig. S1) resembles that of a flow reactor, except for a much smaller surface to volume ratio. Residence times are of the order of hours compared to the typical time scale of minutes in flow reactors.

Reactant and sampling gasses are fed through the insulating walls on opposite sides and provide numerous ports for injection and sampling. The chamber was operated in a constant-flow mode where dry air and reactants were flushed into the chamber constantly using mass flow controllers. A LabView computer program read a differential pressure transmitter (model 5266, Gems Sensors) and triggered an exhaust valve with a high volume pump (VT4.16, Becker) in line in order to restore nominal pressure. The chamber was always operated at slight overpressure (relative to ambient), and the exit valve closed and opened at 2.5 and 3.5 Pa respectively. This range in pressure difference defined a cycle (exit valve open-close-open) that usually took some minutes. The change in flow patterns due to the pressure regulation and the orientations of the inlet tubings (see Fig. S1 ensured turbulent mixing. All connections that supply the chamber were made of stainless steel, except for the differential pressure sensor line (made of Teflon).

On the inlet side, in house air was dried (SP 14, VarioDry) and cleaned of particulate matter and oil mist (F64L, Norgren) before being fed into the chamber and any other parts of the setup. In the VOC injection system, a syringe pump (NE-300, New Era Pump Systems Inc.) continuously injected a mixture of α-pinene and 1-butanol or a mixture of α-pinene and cyclohexane into a warmed glass bulb. A flow of air carried the evaporate from the glass bulb into the chamber. The speed of the syringe

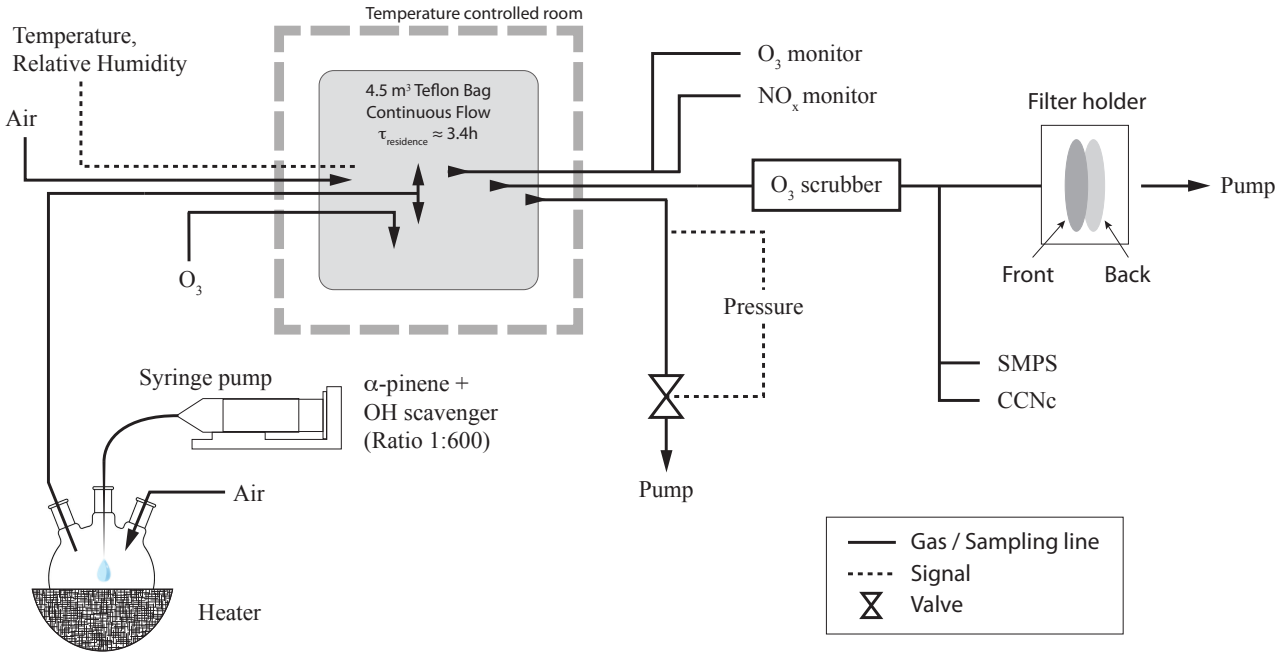

Figure S1. Sketch of the experimental setup of the constant-flow smog chamber. A 4.5 m^3 teflon bag is suspended in a temperature controlled room. Controlled flows of air and the reactants (VOC + OH scavenger, ozone) are constantly fed into the chamber, while a pressure-induced control program opens and closes a valve to the exhaust pump in order to restore ambient pressure. Temperature, RH, and NO_x and ozone levels are monitored. A filter holder with two filters (front and back) is placed in parallel with an SMPS and a CCN counter (CCNC) after an ozone scrubber. The chamber is based on the steady state design of King et al. (2009); Shilling et al. (2008) and Kleindienst et al. (1999).

pump and the total flow defined the VOC concentration inside the bag. The VOC injection system gave rise to minor fluctuations in the VOC concentrations due to bubbles forming in the syringe.

The total inlet flow consisted of 20 L/min dry air, 2 L/min α-pinene + OH scavenger in air and 0.1 L/min ozone-rich air. Under these conditions, the (nominal) residence time was $\tau_{\mathrm{nominal}} = 3.4\,\mathrm{h}$, which is long compared to the open-close cycle of the pressure regulation system. τ_{nominal} was confirmed during simple dilution experiments. The flows (and therefore the residence time inside the chamber) were kept constant during all experiments described here.

Prior to experiments, the chamber was cleaned at 40 °C by flushing with 20 L/min of dry, clean air and high ozone concentrations (ca. 200 ppb) until the total particle concentration was below 1 cm^{-3} for at least 12 h. Once the VOC injection was started, the setup was running for several days without interruption.

S2 Chamber aerosol characterisation

Figure S2 shows the temporal evolution of SMPS-derived size-distributions and an estimate for total mass concentration, $M_{\mathrm{total}}^{\mathrm{SMPS}}$, derived by assuming spherical particles with a density of 1.2 g/cm^3 (Zelenyuk et al., 2008). The charge-correction was not applied to these number-size distributions because the distribution tail at large diameters was beyond the SMPS cut-off diameter. This caused artefacts when applying the charge correction. After the start of VOC-injection, an initial population of particles is formed that grows continuously to sizes of several hundred nanometers within the first hours of the experiment. Multiple populations become visible in Fig. S2 after ca. 5 h that are likely artefacts of multiply-charged particles. As the initial population is growing, it leaves the 'field of view' of the SMPS. As the large particles of the first generation are flushed out of the chamber, less surface area is available for condensation of oxidised vapours and new particle formation is again favoured (at ca. 7 h after start of VOC injection). Roughly one day after injection, new particle formation, condensation upon existing particles, wall losses and the flux of species in and out of the bag are in equilibrium and the measured size distributions stay nearly constant for several days.

Fluctuations in the total mass of the aerosol population (e.g. around 50 h after injection) are most likely due to variations in the VOC injection system. Temporal variability in the size-distribution data originates partly from the fact that no seed particles were present, but such temporal changes in the size-distribution average out over long sampling periods. Panel a in Fig. S3 shows that the SMPS-derived aerosol size distributions is relatively constant over the full sampling time of filters C1f and C1b. The two different OH scavengers (experiments A and B) show very similar mass concentrations and the size distributions share the same shape (not shown).

Panel b in Fig. S3 shows how the generated aerosol particles perform as cloud condensation nuclei. CCN measurements were performed as described previously (King et al., 2012). In short, the aerosol is simultaneously characterized by an SMPS and a CCNC system. The CCNC system itself consists of a DMA, that provides a mono disperse aerosol population for the CCNC and a CPC. The CCNC counts the activated number of particles while the CPC counts the total particle concentration. An automated program allows scanning over the DMA dry diameter and the supersaturation in the CCNC. At each supersaturation, a CCN activity curve is obtained that plots the activated fraction of the aerosol (the ratio of activated aerosol over total concentration) versus the dry diameter of the DMA. Using the size-distribution measured by the SMPS, an inversion is run in order to fit the activity curve (considering multiple charges) and to determine the critical dry diameter, i.e. the size at which particles will activate to be CCN at the given supersaturation. Finally, the program steps through a number of supersaturations in the CCNC in order to derive a curve like the one presented in Panel b in Fig. S3, where for each supersaturation, the critical dry diameter is given.

S3 Back filters

Figure S4 compares the chemical composition of front and back filters C1f and C1b. Panel a shows the ratio between the ion concentration on back and on front filters for each ion. Ratios close to one are observed for high desorption temperatures, such as shown for 350 °C. The lowest ratios are observed for 150 °C indicating that most ions are more abundant during

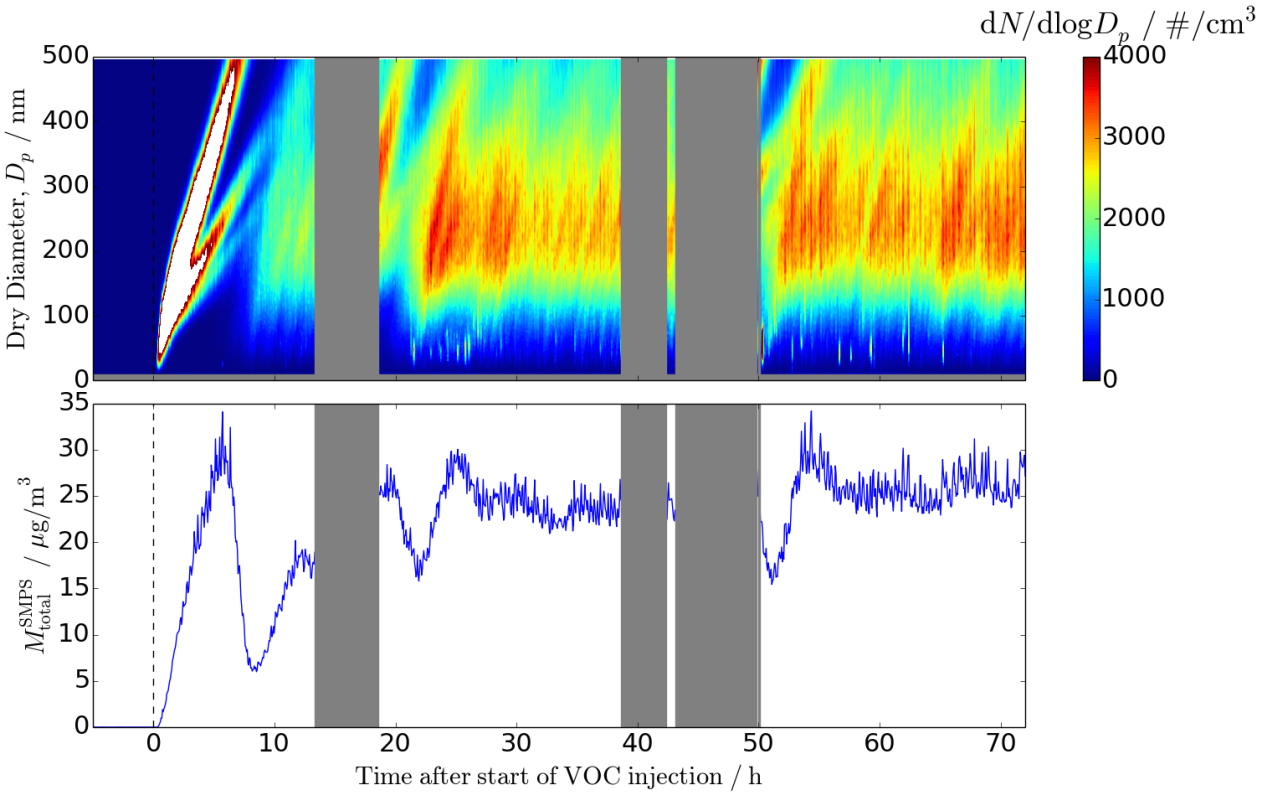

Figure S2. SMPS number size-distribution (10-500 nm range) in #/cm^3 and total mass concentration, $M_{\text{total}}^{\text{SMPS}}$, plotted versus time (for experiment B). Time zero corresponds to the start of VOC injection into the chamber. Filters C1f and C1b sampled between ca. 18 and 42 h and filters C2f and C2b between ca. 48 and 72 h. The SMPS cut-off diameter of 500 nm excludes larger particles, making $M_{\text{total}}^{\text{SMPS}}$ a lower limit. The grey areas denote times when the instrument was offline. The white patch in the initial particle bloom is off the colour scale with values up to 4950 /cm^3.

front filter desorption than during back filter desorption. Ratios for specific compounds are also listed in Table 4 in the main manuscript showing that ions desorbing from front filter C1f at 150 °C with highest concentration typically desorb with much lower concentrations from back filter C1b.

Panel b in Fig. S4 compares the ranking of the detected ions (according to their concentration) on front and back filters. The rank of an ion from a filter measurement carries information about the relative abundance of the ion, independent of the total concentration on that filter. Plotting the back filter rank of an ion versus its rank on the front filter shows whether that ion contributes similarly to the overall mass on both filters. If most ions rank similarly on both filters a high correlation is expected, whereas if the ions contribute differently to the total mass a low correlation is expected. The correlation of ranks of filters C1b and C1f give regression coefficients (R^2) of 0.47 (100 °C), 0.37 (150 °C) and 0.82 (350 °C), respectively.

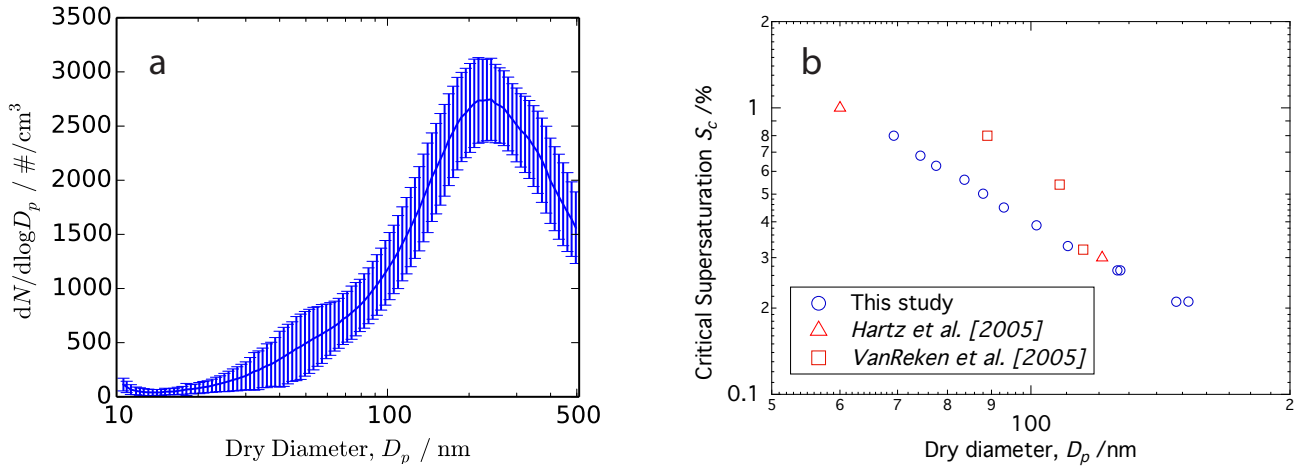

Figure S3. Characterisation of generated aerosol. Panel a shows the average size-distribution and 1-σ standard deviation of the aerosol inside the chamber detected by SMPS during sampling of filters C1f and C1b. Panel b shows the CCN activity measured for experiment A. The CCN activity of the generated SOA in the chamber is in agreement with literature data (Hartz et al., 2005; VanReken et al., 2005).

The low correlation of the ion rankings and the low ion concentration ratios indicate that the material desorbed from the back and front filters at 150 °C differs in chemical composition. The difference in chemical composition complements the large difference in total desorbed mass (Fig. 2 in the main manuscript) and strengthens the conclusion that ions detected from front filter desorption represent aerosol compounds and that ions detected from back filter desorption represent gas-phase compounds. Gas phase compounds adsorb on both front and back filters during sampling (positive gas-phase artefact). After a few hours of sampling, adsorption and re-evaporation are in equilibrium. The gas-phase artefact will remain constant once the equilibrium is reached, while aerosols are still accumulating over time on the front filter driving the division in concentration and chemical composition.

The correlation of the ion rankings and the ion concentration ratios highlight that the chemical composition of compounds desorbing from front and back filters is more similar at 100 °C than for compounds desorbing at 150 °C. Compounds desorbing at 100 °C include the most volatile fraction of aerosols that is partly lost during sampling (negative aerosol artefact). Even though the negative sampling artefact decreases the difference between front and back filters in chemical composition and total mass detected at 100 °C, aerosol compounds constitute the largest fraction of the ion concentration detected at 100 °C on the front filter.

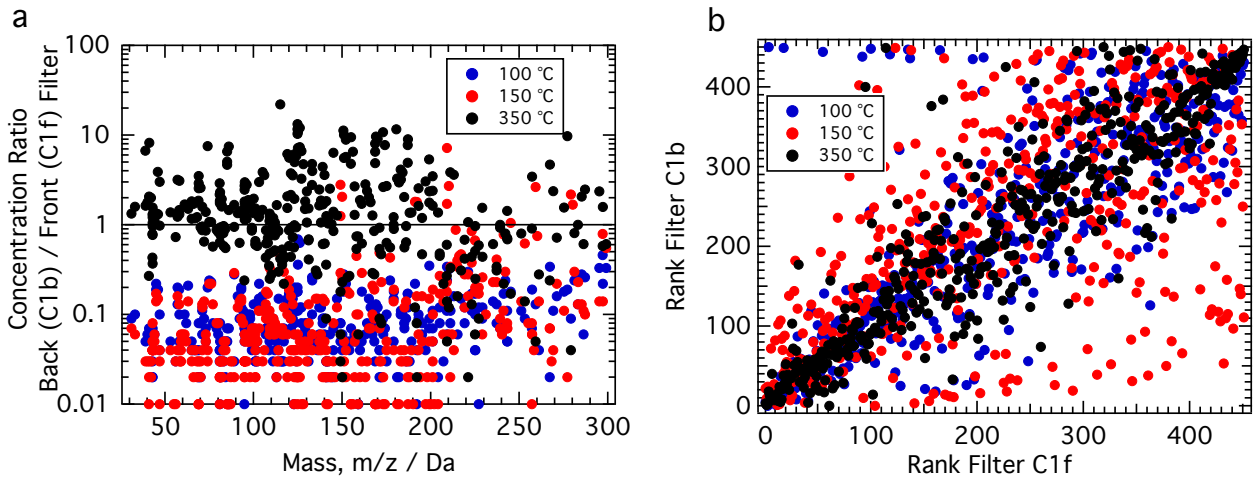

Figure S4. Comparison of back and front filters. Panel a shows the concentration ratio of back filter C1b to front filter C1f for three desorption temperatures. Only ions with mass below 300 Da are shown. Note the logarithmic axis. Panel b compares the relative abundance of ions from filter C1b to their relative abundance on filter C1f by correlating the concentration rankings of ions (largest concentration is ranked highest). The correlation is shown for three desorption temperatures (same color code as Panel a). Linear fits (not shown) to data in Panel b give regression coefficients (R^2) of 0.47 (100 °C), 0.37 (150 °C) and 0.82 (350 °C).

S4 Notes on PTR-MS data

S4.1 Fragmentation in the PTR-MS

Fragmentation of compounds in the PTR-MS is a common artefact (e.g., Holzinger et al., 2010). When such fragmentation occurs, only charged fragments are detected. Protonated water is a common fragment but cannot be observed due to the large background of the primary H_3O^+ ions (19.013 Da). The formation of undetected water means that some oxygen escapes detection, which lowers the reported O:C ratio. If the charged fragments do not coincide in mass with a primary ion at least one of the fragments will be detected by the PTR-MS.

The arrows in the mass spectrum in Fig. 4 indicate pairs of peaks with a mass difference of 14.016 Da (light arrow) and 18.011 Da (dark arrow). The former can be associated with a CH_2 group while the latter corresponds to the mass of a water molecule. When multiple water molecules are lost this produces series of molecules that are connected this way. In one series ions can originate from the same parent compound entering the PTR-MS. In that case these ions show similar thermograms (similar relative concentrations at different temperature steps). This is the case for the ions the dark arrow connects - the large peak at 169.085 Da and the smaller one at 187.097 Da. The ion concentrations differ by a factor of ca. 10, but their thermograms are similar, which indicates that the actual compound desorbing from the filter has a mass of 187.097 Da. The peak at 169.085 Da becomes amplified because of the favoured loss of a water molecule. Ions that are part of a series of the

H_2O-loss fragmentation pattern can be numbered relative to each other as $\pm n \times 18.011\,\mathrm{Da}$. Table 4 and Sect. S6 lists the number n for members of the same series.

Besides the fragmentation that forms water, other fragmentation patterns can occur as well in the PTR-MS. Fragmentation depends on the applied E/N value (Tani et al., 2003; Cappellin et al., 2012), where E is the electric field strength and N the buffer gas number density. E/N describes the drift tube conditions in the PTR-MS and is given in units of Td ($1\,\mathrm{Td} = 1\,\mathrm{Townsend} = 10^{-17}\,\mathrm{Vcm^2mol^{-1}}$). Under the employed conditions ($E/N = 124.4\,\mathrm{Td}$) significant fragmentation is expected for instance for pure gaseous compounds (Tani et al., 2003).

S4.2 Resolution and discrimination of peaks reported in the literature

The high mass resolution of the PRT-ToF-MS used in the present study allows more detailed interpretation of the results compared to previous low resolution data obtained with a quadrupole MS. In particular, the PTR-ToF-MS has not been used for measuring the particulate constituents of α-pinene ozonolysis before whereas quadrupole PTR-MS instruments have been used for monitoring the gas-phase (Shilling et al., 2008; Lee et al., 2006) of SOA chamber experiments. These results are difficult to compare, since partitioning coefficients are not known for many organic compounds. The ion with the highest concentration in this study at 169.085 Da will serve as an example: A low resolution peak at 169 Da might be associated with pinonaldehyde ($C_{10}H_{16}O_2H^+$), one of the main gas-phase oxidation products of the first reaction step in α-pinene ozonolysis (Camredon et al., 2010). However, the precise molecular weight of pinonaldehyde counting all atoms as primary isotopes, ^{12}C, ^{1}H and ^{16}O, is 169.123 Da, which differs significantly from the detected peak at 169.085 Da, and thus the compound is not pinonaldehyde. This finding is in line with the low partitioning coefficient reported for pinonaldehyde (Jenkin, 2004) that prevents it from condensing at room temperature. Literature references that reported compounds other than what was identified in this study at the same masses are therefore given in brackets in Table 4 and Sect. S6.

S4.3 Mass scale

As noted earlier the ion at 169.085 Da appears to be in the same water series as the ion with mass 187.097 Da. Besides mechanistic implications, these water series prove useful in checking the performance of the PTR-MS: The presence of water series at high and low masses (e.g. the primary ion and its water clusters and the pair at 169.085 Da and 187.097 Da) ensures that drift in the autoscaling of the PTR-MS mass scale does not cause any ions to be associated with the wrong mass. If the instrument had shown a drift in the mass scale, the drift would scale with the detected mass: a larger deviation would result for heavier ions. However, since the exact difference of the mass of water (18.011 Da) is found on both ends of the mass spectrum, this systematic error can be excluded. Therefore, the given peak assignment is believed to be accurate.

S4.4 Charring

When organic material is heated it pyrolyzes, producing char and gas phase fragments including CO and CO_2, a process commonly referred to as charring. Charring is a known interference with filter-based thermogram methods (Holzinger et al.,

2010). The electron affinities of CO and CO_2 are lower than that of water and hence no peaks are detected at the corresponding masses in the PTR-MS. Charring may therefore bias the measurements with implications that include lowered O:C ratios.

S5 Position-specific isotope measurements

Quantitative nuclear magnetic resonance spectrometry (NMR) tuned for isotopic measurement is a tool for quantifying each isotopic isomer of a given molecule (isotopomers): ^{2}H (Martin et al., 2006a, b) or ^{13}C (Caytan et al., 2007b). The latest technique, irm-^{13}C NMR, is a recent advancement on the more well established irm-^{2}H NMR (Singleton and Thomas, 1995). It is more of a challenge to quantify the range of variation of ^{13}C in natural compounds, which is about ten times less for ^{13}C than ^{2}H (about 50 ‰ and 500 ‰, respectively, on the δ-scale). The realization of the method required establishing ^{13}C NMR conditions to attain a precision of 1 ‰.

S5.1 NMR acquisition conditions

Table S1 summarises the NMR acquisition parameters used for isotopic ^{13}C-NMR. The offset for both ^{13}C and ^{1}H was set at the middle of the frequency range observed. An inverse-gated decoupling technique was used to avoid any Nuclear Overhauser Effect and a cosine adiabatic pulse with appropriate phase cycles was employed as proton decoupling sequence (Tenailleau and Akoka, 2007). A repetition time/inter-pulse delay, greater than ten times the longest longitudinal relaxation delay, T_1, of the compound was used and the acquisition parameters were adjusted to obtain a signal-to-noise ratio (SNR) > 1500. Free induction decay was submitted to an exponential multiplication inducing a line broadening of 2 Hz. The curve fitting was based on a total-line-shape analyses (deconvolution) carried out with a Lorentzian mathematical model using Perch Software (Perch™ NMR Software, http://www.perchsolutions.com). From previous experiments (Bayle et al., 2014; Caytan et al., 2007), SNR > 1500 usually leads to a standard deviation for precision of around 0.2 ‰. Five spectra were recorded for each measurement: the values reported for each carbon are the mean of the five spectra.

S5.2 Intramolecular ^{13}C composition calculations

Briefly, the positional isotopic distribution in a molecule was obtained from the ^{13}C mole fractions f_i (where i stands for the C-atom position considered) as follows: $f_i = S_i/S_{\mathrm{tot}}$, where S_i is the ^{13}C-signal (i.e. the area under the peak associated with the C-atom at position i, Fig. S5) and S_{tot} is the sum of all ^{13}C-signal areas of the molecule. Each S_i was corrected to compensate for the slight loss of intensity caused by satellites (^{13}C-^{13}C interactions) by multiplying by $(1 + n \times 0.011)$, where n is the number of carbon atoms directly attached to the C-atom position i and 1.1 % (= 0.011) is the average natural ^{13}C-abundance (see (Silvestre et al., 2009) for a detailed explanation). If F_i denotes the statistical mole fraction (homogeneous ^{13}C-distribution) at any C-atom position i, then the position-specific relative deviation in the ^{13}C-abundance is $d_i = f_i/F_i - 1$. The values of d_i were converted to delta-values (in ‰) using the isotope composition of the whole molecule, $\delta^{\circ}_{\mathrm{TC}}(^{13}\mathrm{C})$, obtained by IR-MS. Thus, the position-specific compositions are expressed as $\delta_i(^{13}\mathrm{C})$ for each C-atom position of the molecule. Since

Table S1. NMR acquisition parameters used for isotopic ^{13}C-NMR. T_1 is the longitudinal relaxation delay after addition of the relaxing agent.

Acquisition	Spectral width /ppm	238
	^{13}C offset frequency /ppm	110
	^{1}H decoupling offset /ppm	4
	Inter-pulse delay /s	32
FID treatment	Line-broadening /Hz	2
T_1 /s	C_1	3.0
	C_2	2.4
	C_3	2.8
	C_4	2.5
	C_5	3.2
	C_6	2.2
	C_7	2.2
	C_8	2.3
	C_9	2.2
	C_{10}	2.3

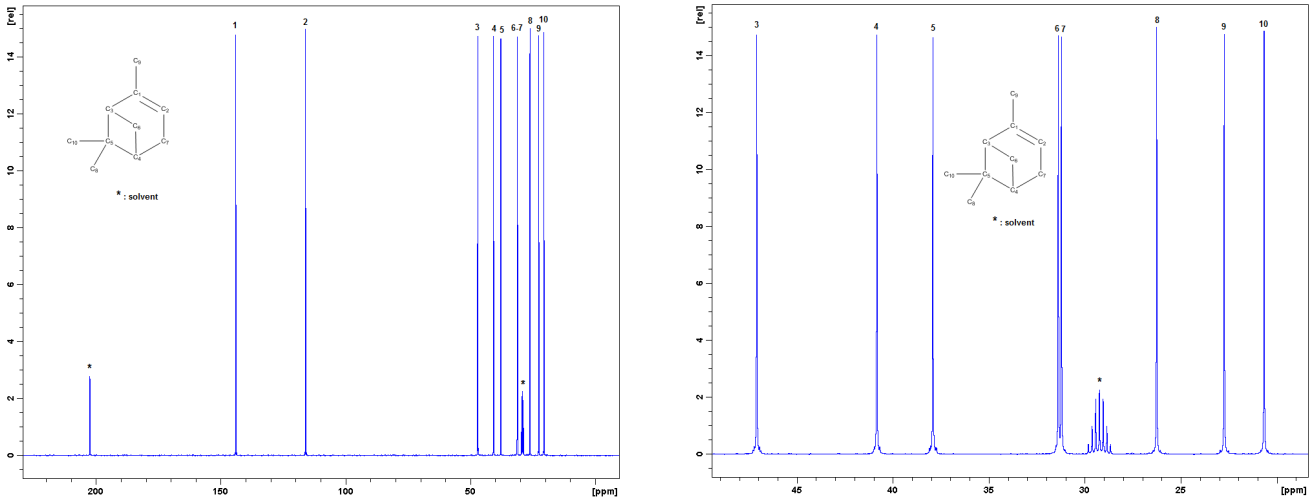

Figure S5. ^{13}C NMR spectrum of α-pinene in acetone-d_6. Left pane: full spectrum, right pane: zoom. The carbon atoms are numbered in relation to decreasing ^{13}C chemical shift in the ^{13}C NMR spectrum.

the peaks of C-6 and C-7 are very close in the ^{13}C NMR spectrum (right panel in Fig. S5), the average of the two corresponding $\delta_i\left(^{13}\mathrm{C}\right)$ values is given for both. Table S2 shows the discussed quantities for one NMR spectrum of the present data set.

Table S2. Example calculation of $\delta_i\left(^{13}\mathrm{C}\right)$ of α-pinene from the peak areas in one ^{13}C NMR spectrum. Corrected areas take the interference from satellites into account. See text for more details. Calculations are based on a global ^{13}C/^{12}C ratio of 0.010808 corresponding to $\delta^{\circ 2}_{\mathrm{TC}}\left(^{13}\mathrm{C}\right) = -27.7‰$ with respect to the VPDB scale as measured by IR-MS.

	C_1	C_2	C_3	C_4	C_5	C_6	C_7	C_8	C_9	C_{10}
Area /a.u.	355.40	360.80	353.30	354.60	347.50	362.50	360.50	361.20	358.60	359.60
Corrected area	367.13	368.74	364.96	366.30	362.79	366.49	364.47	365.17	362.54	363.56
f_i	0.1005	0.1010	0.0999	0.1003	0.0993	0.1003	0.0998	0.1000	0.0993	0.0995
F_i	1/10	1/10	1/10	1/10	1/10	1/10	1/10	1/10	1/10	1/10
f_i/F_i	1.0052	1.0097	0.9993	1.0030	0.9934	1.0035	0.9980	0.9999	0.9927	0.9955
$\delta_i\left(^{13}\mathrm{C}\right)/‰$	-22.5	-18.2	-28.3	-24.7	-34.2	-24.2	-29.7	-27.8	-34.8	-32.1

S6 Full list of ions (filter C1f)

The full list of ions detected by PTR-MS from compounds desorbing from filter C1f is printed here and can also be found in the complimentary .csv file 'SI_filter_C1f.csv'.

SI to C. Meusinger et al. ***Chemical and isotopic composition of secondary organic aerosol generated by alpha-pinene ozonolysis***

Full list of ions detected by PTR-MS from compounds desorbing from filter C1f ranked by their concentration

Rank	m/z	Formula	Maximum concentration /ng/m3	Desorption Temp. of max. conc. /°C	Description	Literature	H2O relatives
1	169.085	C9H12O3H+	267.79	150		a, (c, d)	+1 (187.093 Da, #72), -1 (151.076 Da, #22), -2 (133.065 Da, #202)
2	81.07	C6H8H+	257.57	150	similar to 95.086 Da (#8)		+1 (99.08 Da, #32)
3	125.096	C8H12OH+	221.48	150			
4	43.0172	C2H2OH+	149.37	150		a	
5	39.0226	C3H2H+	132.93	150			
6	155.07	C8H10O3H+	127.41	150		a, (b, d)	+1 (173.081 Da, #13)
7	41.0381	C3H4H+	111.32	150		(a)	
8	59.0491	C3H6OH+	110.01	150	Acetone	a, b, c	
9	95.0861	C7H10H+	107.5	150	similar to 81.07 Da (#1)	(d)	
10	127.075	C7H10O2H+	69.69	150		a, c	
11	83.0496	C5H6OH+	66.57	150		(a), c	+1 (101.06 Da, #62), -1 (65.04 Da, #96)
12	107.086	C8H10H+	64.79	150		(a)	
13	173.079	C8H12O4H+	58.75	150	norpinic acid	b, e, g, (b, e)	-1 (155.07 Da, #6)
14	45.033	C2H4OH+	58.56	100	Acetaldehyde	a, b, c	+1 (63.043 Da, #336)
15	85.065	C5H8OH+	56.71	150			
16	141.054	C7H8O3H+	56.22	150		a, b, c	+1 (159.065 Da, #63)
17	123.081	C8H10OH+	53.69	150		(a), b, c	-1 (105.072 Da, #58)
18	67.0546	C5H6H+	50.57	150		(d)	
19	69.0337	C4H4OH+	49.81	150		(a)	
20	69.0699	C5H8H+	43.6	150		(a)	
21	171.065	C8H10O4H+	42.34	150	small peak nearby unresolved (norpinonic acid?)	a, c, (e, f, g)	-1 (153.055 Da, not listed)
22	151.076	C9H10O2H+	42.12	150		(a)	+1 (169.085 Da, #1), +2 (187.093 Da, #72), -1 (133.065 Da, #202)
23	85.029	C4H4O2H+	40.88	200		c	
24	153.091	C9H12O2H+	39.97	150		c, (g)	-1 (135.081 Da, #59), -2 (117.070 Da, #152)
25	141.089	C8H12O2H+	39.91	150	2,2-Dimethyl-cyclobutyl-1,3-diethanal	a, b, c, g, (g)	
26	71.049	C4H6OH+	39.63	150	MUK & MACR	(a), b	
27	115.076	C6H10O2H+	37.17	150		a	-1 (97.0655 Da, #30)
28	181.084	C10H12O3H+	36.81	150			+1 (199.095, #67), +2 (217.107 Da, #310), -1 (163.076 Da, #107)
29	55.0534	C4H6H+	35.56	150			+1 (73.065 Da, #88)
30	97.0655	C6H8OH+	29.16	150		a	+1 (115.076 Da, #27)
31	170.089	13CC8H12O3H+	27.96	150	13C of #2	(a)	+1 (188.096, #219), -1 (152.080, #120), -2 (unresolved)
32	99.0807	C6H10OH+	27.48	150		(a)	-1 (81.07 Da, #2)
33	165.09	C10H12O2H+	26.62	350		a	
34	79.0547	C6H6H+	26.36	150		a	
35	57.0698	C4H8H+	26.3	150			
36	183.099	C10H14O3H+	26	150	C10$CO, 4-Oxopinonaldehyde	a, e, f, g, h	+1 (201.117 Da, #239), +2 (not resolved)
37	83.085	C6H10H+	25.48	150		(a)	
38	109.101	C8H12H+	25.45	150			
39	125.06	C7H8O2H+	25.36	150		a, c	not well resolved
40	151.111	C10H14OH+	24.1	150			
41	139.04	C7H6O3H+	22.68	150		a, c	+1 (157.05 Da, #50)
42	93.0697	C7H8H+	21.98	150			
43	109.066	C7H8OH+	21.75	150			
44	126.099	13CC7H12OH+	20.59	150			
45	57.0337	C3H4OH+	20.41	100		c	+1 (75.044 Da, #48)
46	47.0126	CH2O2H+	19.99	150		a, c	
47	95.0576	C5H6N2H+	19.81	150			
48	75.044	C3H6O2H+	19.79	100		a	-1 (57.033 Da, #45)
49	129.055	C6H8O3H+	19.64	150		a, c	
50	157.05	C7H8O4H+	18.8	150	CO235C6CHO	c, h	-1 (139.04 Da, #41)
51	171.098	13CC11H11NH+	18.75	150	norpinonic acid (?), C9H14O3H+	f, g	
52	119.085	C9H10H+	17.71	150			
53	143.07	C7H10O3H+	17.46	200		a, c	
54	167.104	C5H14O4N2H+	17.17	150			+1 (185.118 Da, #116), -1 (149.098 Da, #134)
55	123.114	C9H14H+	15.99	150			
56	139.075	C8H10O2H+	15.98	150		a, c	-1 (121.068, #101), +1 (157.087, #64)
57	113.06	C6H8O2H+	15.96	150		a, b, c	
58	105.071	C8H8H+	15.86	150		b	+1 (123.081 Da, #17)
59	135.081	C9H10OH+	15.02	150			+1 (153.091 Da, #24), -1 (117.070 Da, #152)
60	61.0286	C2H4O2H+	14.8	150	Acetic acid	c	
61	87.0445	C4H6O2H+	14.59	150		a, c	
62	101.06	C5H8O2H+	14.4	150		c	-1 (83.0496 Da, #11), -2 (65.04 Da, #96)
63	159.065	C7H10O4H+	14.27	150	C811OH	b, h	-1 (141.054 Da, #16)
64	157.083	C8H12O3H+	13.94	150	C721CHO	h	-1 (139.075 Da, #56), -2 (121.068 Da, #101)
65	111.08	C7H10OH+	13.8	150		a, b	
66	55.0182	C3H2OH+	13.36	150			
67	199.093	C5H14O6N2H+	12.87	150	oxopinonic acid, keto-pinonic acid	e, g	-1 (181.084 Da, #28), -2 (163.076 Da, #107), +1 (217.107 Da, #310)
68	82.0738	13CC5H8H+	12.15	150			
69	156.074	13CC7H10O3H+	11.91	150			
70	145.05	C6H8O4H+	11.9	150		b	
71	111.045	C6H6O2H+	11.87	150		a, b, c	
72	187.093	C9H14O4H+	11.37	150	pinic acid, 10-OH norpinonic acid, PINIC	e, f, g, h	-1 (169.085 Da, #1), -2 (151.076 Da, #22), -3 (133.065 Da, #202)
73	95.0497	C6H6OH+	11.09	150			-1 (77.040, #213)
74	139.109	C9H14OH+	10.82	150	nopinone (?)	a, f	-1 (121.103 Da, #100)
75	81.0353	C5H4OH+	10.49	150			
76	97.058	no match	10.35	150			
77	137.095	C9H12OH+	9.87	150			
78	111.053	C5H6ON2H+	9.67	150		a	
79	73.0283	C3H4O2H+	9.43	150		a, c	
80	113.024	C5H4O3H+	9.18	200		a, b, c	-1 (95.020 Da, #144)
81	53.0385	C4H4H+	8.95	150			
82	99.0444	C5H6O2H+	8.83	150		c	
83	96.09	13CC6H10OH+	8.82	150			

Rank	m/z	Formula	Maximum concentration /ng/m3	Desorption Temp. of max. conc. /°C	Description	Literature	H2O relatives
84	137.06	C8H8O2H+	8.23	150			
85	109.058	C2H8O3N2H+	8.16	150			
86	93.062	no match	8.11	150			
87	129.087	no match	8.06	150		a	
88	73.0648	C4H8OH+	8.05	150		a	-1 (55.0534 Da, #29)
89	99.0085	C4H2O3H+	8.01	200			
90	128.078	13CC6H10O2H+	7.65	150			
91	68.9974	no match	7.56	150			
92	95.042	no match	7.51	150			
93	214.087	C13H11O2NH+	7.45	150			
94	167.071	C9H10O3H+	7.33	150			
95	97.0292	C5H4O2H+	7.33	150		a, c	
96	65.039	C5H4H+	7.32	150			+1 (83.0496 Da, #11), +2 (101.06 Da, #62)
97	123.052	no match	7.27	150			
98	197.079	C10H12O4H+	7.23	150			
99	173.147	no match	6.88	150			
100	121.101	C9H12H+	6.86	150			+1 (139.109 Da, #74)
101	121.065	C8H8OH+	6.86	150			+1 (139.075 Da, #56), +2 (157.080, #64)
102	127.037	C6H6O3H+	6.62	150		c	
103	85.0993	C6H12H+	6.44	150			
104	651.119	no match	6.37	150			
105	185.079	C9H12O4H+	6.35	150		c	
106	725.102	no match	6.26	150			
107	163.075	C10H10O2H+	5.95	150		b	+1 (181.084 Da, #28), +2 (199.095, #67), +3 (217.107 Da, #310)
108	82.0718	13CC5H8H+	5.95	150			
109	124.084	13CC7H10OH+	5.84	150			
110	108.089	13CC7H10H+	5.8	150			
111	91.0549	C7H6H+	5.76	150			
112	125.023	C6H4O3H+	5.67	150			
113	174.083	13CC7H12O4H+	5.67	150	C8902	h	
114	107.049	C7H6OH+	5.42	150			
115	33.0327	CH4OH+	5.32	150	Methanol		
116	185.117	C10H16O3H+	5.31	150	pinonic acid, OH-pinonaldehyde, PINONIC, C107OH, C109OH	a, e, f, g, h	-1 (167.105 Da, #54), -2 (149.098 Da, #134)
117	172.068	13CC7H10O4H+	5.1	150			
118	101.052	no match	4.77	150			
119	142.058	13CC6H8O3H+	4.69	150			
120	152.079	13CC8H10O2H+	4.54	150			+1 (170.089, #31), +2 (188.096, #219), -1 (unresolved)
121	171.148	C9H18ON2H+	4.49	150			
122	43.0536	C3H6H+	4.47	150			
123	115.04	C5H6O3H+	4.4	150		a, c	
124	40.0256	13CC2H2H+	4.29	150			
125	154.093	13CC8H12O2H+	4.29	150			
126	182.088	13CC9H12O3H+	4.28	150			+1 (200.097 Da, #197), +2 (218.109 Da, not resolved)
127	70.0734	13CC4H8H+	4.12	150			
128	71.0812	no match	4.06	150			
129	60.0521	13CC2H6OH+	4.02	150			
130	123.043	C7H6O2H+	3.99	150			
131	183.163	no match	3.95	150			
132	141.003	C2H4O7H+	3.94	150			
133	84.0525	13CC4H6OH+	3.88	150			
134	149.095	C10H12OH+	3.84	150	methylchavicol (Holzi2005)	b	+1 (167.105, #54), +2 (185.118 Da, #116)
135	211.093	C6H14O6N2H+	3.81	150			
136	42.0414	13CC2H4H+	3.72	150			
137	142.093	13CC7H12O2H+	3.65	150			
138	741.107	no match	3.62	150			
139	121.093	no match	3.54	150			
140	44.0205	13CCH2OH+	3.31	150			
141	653.119	no match	3.28	150			
142	86.068	13CC4H8OH+	3.28	150			
143	184.103	13CC9H14O3H+	3.22	150			
144	95.0141	C5H2O2H+	3.2	200		b	+1 (113.024 Da, #80)
145	145.089	no match	3.16	150			
146	166.094	13CC9H12O2H+	3.13	350			
147	87.0796	C5H10OH+	3.02	150	MBO (holzi 2005)	a, b	
148	109.031	C6H4O2H+	2.96	150			
149	101.095	C6H12OH+	2.95	150			
150	99.0371	no match	2.95	150			
151	101.024	C4H4O3H+	2.95	150		c	
152	117.069	C9H8H+	2.87	150			+1 (135.081 Da, #59), +2 (153.091 Da, #24)
153	103.04	C4H6O3H+	2.86	100			
154	152.112	13CC4H14O3N2H+	2.85	150			
155	149.024	C8H4O3H+	2.83	150		c	
156	110.069	13CC6H8OH+	2.6	150			
157	96.0531	13CC5H6OH+	2.57	150			
158	126.063	13CC6H8O2H+	2.54	150			
159	429.077	no match	2.5	150			
160	68.058	13CC4H6H+	2.48	150			
161	83.0138	C4H2O2H+	2.47	150			
162	42.9985	no match	2.43	150			
163	147.08	C10H10OH+	2.41	150			
164	110.105	13CC7H12H+	2.35	150			
165	103.048	C3H6O2N2H+	2.34	100			
166	70.038	13CC3H4OH+	2.3	150			
167	116.08	13CC5H10O2H+	2.27	150			
168	71.0136	C3H2O2H+	2.27	200			

Rank	m/z	Formula	Maximum concentration /ng/m3	Desorption Temp. of max. conc. /°C	Description	Literature	H2O relatives
169	55.0103	no match	2.24	150			
170	652.095	no match	2.24	150			
171	187.068	no match	2.23	150			
172	72.052	13CC3H6OH+	2.23	150			
173	94.0733	13CC6H8H+	2.23	150			
174	667.131	no match	2.22	150			
175	117.061	no match	2.22	150		a	
176	133.097	C5H12O2N2H+	2.18	150			
177	215.09	C10H14O5H+	2.15	150			
178	652.128	no match	2.11	150			
179	187.06	C8H10O5H+	2.11	200			
180	98.0687	13CC5H8OH+	2.1	150			
181	93.0396	C6H4OH+	2.08	150			
182	168.107	13CC9H14O2H+	2.02	150			
183	31.017	CH2OH+	2.01	150	Formaldehyde		
184	100.084	13CC5H10OH+	1.98	150			
185	119.05	C8H6OH+	1.87	150			
186	86.0328	13CC3H4O2H+	1.87	200			
187	140.044	13CC6H6O3H+	1.86	150			
188	120.088	13CC8H10H+	1.85	150			
189	168.676	no match	1.83	150			
190	124.819	no match	1.81	150			
191	159.131	no match	1.79	150			
192	239.23	no match	1.77	150			
193	229.102	C6H16O7N2H+	1.76	150			
194	56.0575	13CC3H6H+	1.71	150			
195	84.0884	13CC5H10H+	1.71	150			
196	277.137	C11H20O6N2H+	1.68	200			
197	200.097	13CC4H14O6N2H+	1.66	150	C10H15O4H+, C107O2	h	+1 (218.109 Da, not resolved), -1 (182.091 Da, #126)
198	149.062	13CC4H9O4NH+	1.64	150			
199	136.084	13CC8H10OH+	1.63	150			
200	80.0576	13CC5H6H+	1.62	150			
201	119.036	C4H6O4H+	1.61	150			
202	133.065	C9H8OH+	1.6	150		a	+1 (151.076 Da, #22), +2 (169.085 Da, #1), +3 (187.093 Da, #72)
203	654.111	no match	1.57	150			
204	199.161	no match	1.56	150			
205	140.078	13CC7H10O2H+	1.56	150			
206	80.9047	no match	1.56	150			
207	154.934	no match	1.55	150			
208	179.07	C10H10O3H+	1.55	350		b	-1 (161.072, #401)
209	121.028	C7H4O2H+	1.51	150			
210	213.074	C10H12O5H+	1.5	200		b	-1 (195.068 Da, #265)
211	130.058	13CC5H8O3H+	1.49	150			
212	103.083	no match	1.48	200			
213	77.0394	C6H4H+	1.46	150			+1 (95.0497 Da, #73)
214	80.938	no match	1.43	150			
215	106.074	13CC7H8H+	1.43	150			
216	144.073	13CC6H10O3H+	1.42	200			
217	371.092	no match	1.41	150			
218	158.086	no match	1.4	150			
219	188.096	no match	1.39	150	C97O2	h	-1 (170.089, #31), -2 (152.080, #120), -3 (unresolved)
220	179.098	no match	1.37	350			
221	158.053	13CC6H8O4H+	1.36	150			
222	80.9795	no match	1.34	150			
223	46.0305	CH3ONH+	1.33	150			
224	59.0089	no match	1.32	150			
225	669.137	no match	1.27	150			
226	257.246	C16H32O2H+	1.27	150			
227	223.097	C12H14O4H+	1.27	150			
228	355.063	no match	1.26	150			
229	145.104	13CC6H13O2NH+	1.26	150			
230	65.022	13CC3HNH+	1.25	150			
231	209.189	C14H24OH+	1.23	100			
232	160.069	13CC6H10O4H+	1.22	150			
233	193.117	C7H16O4N2H+	1.22	150			
234	112.083	13CC6H10OH+	1.2	150			
235	140.114	13CC8H14OH+	1.19	150			
236	285.268	no match	1.17	150			
237	154.926	no match	1.16	150			
238	279.155	C11H22O6N2H+	1.16	200			
239	201.117	no match	1.13	150	C107OOH, C109OOH, HOPINONIC, C108OH, 10-OH pinonic acid, OH-pinonaldehyde	e, f, g, h	-1 (183.099 Da, #36) +1 (not resolved)
240	267.258	no match	1.13	150			
241	80.8614	no match	1.12	150			
242	112.048	13CC5H6O2H+	1.11	150			
243	198.084	13CC9H12O4H+	1.09	150			
244	131.07	C6H10O3H+	1.09	150			
245	189.084	C7H12O4N2H+	1.09	150			
246	114.065	13CC5H8O2H+	1.09	150			
247	101.016	no match	1.09	150			
248	122.104	13CC8H12H+	1.08	150			
249	138.098	13CC8H12OH+	1.06	150			
250	102.062	13CC4H8O2H+	1.05	150			
251	105.036	13CC2H5O3NH+	1.04	150			
252	168.08	C12H9NH+	1.03	150			
253	168.649	no match	0.99	150			

Rank	m/z	Formula	Maximum concentration /ng/m3	Desorption Temp. of max. conc. /°C	Description	Literature	H2O relatives
254	195.095	C6H14O5N2H+	0.98	150			
255	257.226	C19H28H+	0.98	150			
256	80.9714	no match	0.97	150			
257	154.711	no match	0.97	150			
258	124.785	no match	0.96	150			
259	138.066	13CC7H8O2H+	0.94	150			
260	269.165	C17H20ON2H+	0.92	150			
261	82.0405	no match	0.92	150			
262	122.068	13CC7H8OH+	0.9	150			
263	74.0636	no match	0.89	150			
264	133.056	no match	0.89	150			
265	195.068	C10H10O4H+	0.89	200		b	+1 (213.074 Da, #210)
266	131.088	13CC5H11O2NH+	0.89	150			
267	150.726	no match	0.86	150			
268	131.034	C5H6O4H+	0.86	150			
269	201.076	C9H12O5H+	0.84	150			
270	110.993	CH2O6H+	0.83	150			
271	431.076	no match	0.81	150			
272	140.928	no match	0.81	150			
273	578.098	no match	0.79	100			
274	164.077	13CC9H10O2H+	0.78	150			
275	58.072	13CC3H8H+	0.77	150			
276	186.081	13CC3H12O6N2H+	0.76	150			
277	124.794	no match	0.76	150			
278	94.8514	no match	0.76	150			
279	68.97	no match	0.76	150			
280	202.076	13CC3H12O7N2H+	0.75	150			
281	87.01	C3H2O3H+	0.75	150			
282	186.117	no match	0.74	150			
283	241.107	C12H16O5H+	0.74	200			
284	42.9903	no match	0.73	150			
285	94.8927	no match	0.73	150			
286	58.0365	13CC2H4OH+	0.72	100			
287	94.9561	no match	0.71	150			
288	98.0605	C5H7ONH+	0.71	150			
289	150.098	13CC9H12OH+	0.71	150			
290	577.101	no match	0.71	100			
291	146.053	13CC5H8O4H+	0.71	150			
292	66.0437	13CC4H4H+	0.7	150			
293	158.028	13CC4H4O4N2H+	0.69	150			
294	76.0484	13CC2H6O2H+	0.69	100			
295	88.0483	13CC3H6O2H+	0.69	150			
296	204.119	13CC11H14ON2H+	0.68	150			
297	89.0233	C3H4O3H+	0.68	150			
298	219.112	C12H14O2N2H+	0.67	350			
299	124.049	13CC6H6O2H+	0.66	150			
300	116.106	C6H13ONH+	0.66	150			
301	154.685	no match	0.66	150			
302	193.088	13CC6H13O5NH+	0.66	350			
303	108.962	no match	0.66	150			
304	447.088	no match	0.65	150			
305	114.091	C6H11ONH+	0.65	150			
306	211.196	no match	0.64	150			
307	227.123	C7H18O6N2H+	0.64	200			
308	100.047	13CC4H6O2H+	0.63	150			
309	231.095	C9H14O5N2H+	0.63	350			
310	217.107	C10H16O5H+	0.63	350	C108OOH	f, h	-1 (199.095, #67), -2 (181.084 Da, #28), -3 (163.076 Da, #107)
311	58.0803	no match	0.63	150			
312	225.135	C9H20O6H+	0.62	150			
313	577.071	no match	0.62	100			
314	209.109	C14H12N2H+	0.62	150			
315	205.113	no match	0.61	350	C921OOH	h	
316	175.105	C7H14O3N2H+	0.61	150			
317	161.096	C11H12OH+	0.61	350			
318	212.097	13CC5H14O6N2H+	0.61	150			
319	223.119	C9H18O6H+	0.61	150			
320	175.08	13CC6H11O4NH+	0.61	150			
321	201.092	C13H12O2H+	0.61	150			
322	172.15	13CC8H18ON2H+	0.6	150			
323	295.147	C11H22O7N2H+	0.6	200			
324	108.054	13CC6H6OH+	0.6	150			
325	199.17	C12H22O2H+	0.6	150			
326	430.084	no match	0.59	150			
327	140.919	no match	0.59	150			
328	210.117	13CC6H16O5N2H+	0.59	150			
329	94.902	no match	0.59	150			
330	94.9478	no match	0.59	150			
331	130.093	13CC6H12O2H+	0.59	150			
332	45.0065	no match	0.59	100			
333	177.115	C8H16O4H+	0.58	350			
334	229.214	C14H28O2H+	0.57	150			
335	56.021	13CC2H2OH+	0.57	150			
336	63.0429	C2H6O2H+	0.57	150			-1 (45.033 Da, #14)
337	239.137	C12H18O3N2H+	0.57	150			
338	168.668	no match	0.57	150			

Rank	m/z	Formula	Maximum concentration /ng/m3	Desorption Temp. of max. conc. /°C	Description	Literature	H2O relatives
339	207.099	C7H14O5N2H+	0.57	350			
340	225.109	C7H16O6N2H+	0.56	150			
341	114.027	13CC4H4O3H+	0.56	200			
342	190.104	13CC10H12ON2H+	0.56	150			
343	68.9359	no match	0.55	150			
344	89.0603	C4H8O2H+	0.55	150			
345	430.062	no match	0.54	150			
346	579.095	no match	0.54	100			
347	205.089	13CC7H13O5NH+	0.53	350			
348	42.933	no match	0.53	150			
349	146.075	no match	0.53	150			
350	299.063	no match	0.53	150			
351	47.046	no match	0.53	150	etanol		
352	243.129	C12H18O5H+	0.51	150			
353	216.09	13CC4H14O7N2H+	0.51	150	C108O2	h	
354	297.155	C12H24O8H+	0.51	150			
355	117.024	no match	0.5	150		a	
356	243.231	C15H30O2H+	0.5	150			
357	92.0581	13CC6H6H+	0.5	150			
358	209.165	C12H20ON2H+	0.49	100			
359	257.128	C15H16O2N2H+	0.49	150			
360	42.9787	no match	0.49	150			
361	593.15	no match	0.48	100			
362	131.08	C5H10O2N2H+	0.48	150			
363	81.2891	no match	0.48	150			
364	102.092	C5H11ONH+	0.47	150			
365	207.13	no match	0.47	350			
366	98.029	13CC4H4O2H+	0.47	150			
367	267.132	C13H18O4N2H+	0.46	150			
368	41.007	no match	0.46	150			
369	68.0501	C4H5NH+	0.46	150			
370	188.064	13CC7H10O5H+	0.45	150			
371	58.9874	no match	0.45	150			
372	258.25	13CC15H32O2H+	0.44	150			
373	180.64	no match	0.44	150			
374	209.083	13CC6H13O6NH+	0.44	200			
375	215.181	C16H22H+	0.44	150			
376	281.143	C15H20O5H+	0.44	150			
377	225.043	13CC5H9O8NH+	0.43	150			
378	356.068	no match	0.42	150			
379	58.924	no match	0.42	150			
380	45.9922	O2N+	0.42	150			
381	122.804	no match	0.41	150			
382	42.9554	no match	0.41	150			
383	150.028	13CC7H4O3H+	0.4	150			
384	94.837	no match	0.4	150			
385	241.178	C14H24O3H+	0.4	150			
386	112.041	C5H5O2NH+	0.4	150			
387	74.0313	13CC2H4O2H+	0.4	150			
388	42.9091	no match	0.4	150			
389	261.137	no match	0.4	350			
390	225.216	no match	0.39	150			
391	283.147	C17H18O2N2H+	0.39	150			
392	38.9477	no match	0.39	150			
393	357.062	no match	0.39	150			
394	106.83	no match	0.38	150			
395	44.049	C2H5NH+	0.38	150			
396	201.163	C15H20H+	0.37	150			
397	62.0316	13CCH4O2H+	0.36	150			
398	42.0333	C2H3NH+	0.36	150			
399	46.991	O215N+	0.36	150			
400	81.287	no match	0.35	150			
401	161.059	C10H8O2H+	0.35	150			+1 (179.07 Da, #208)
402	58.9788	no match	0.35	150			
403	227.096	C12H18O4H	0.35	150			
404	255.137	C17H18O2H+	0.34	150			
405	251.147	C11H22O6H+	0.34	150			
406	42.9691	no match	0.34	150			
407	243.119	C7H18O7N2H+	0.34	150			
408	43.1766	no match	0.34	150			
409	201.176	no match	0.34	150			
410	297.077	13CC12H13O7NH+	0.34	150			
411	283.24	C16H30O2N2H+	0.34	150			
412	124.041	C6H5O2NH+	0.33	150			
413	240.236	no match	0.33	150			
414	271.14	C10H22O8H+	0.33	150			
415	275.246	C18H30N2H+	0.32	150			
416	237.137	C16H16N2H+	0.32	200			
417	44.0121	CHONH+	0.31	150			
418	40.9457	no match	0.31	150			
419	432.075	no match	0.31	150			
420	194.098	C14H11NH+	0.31	150			
421	448.087	no match	0.3	150			
422	192.104	13CC6H14O4N2H+	0.3	150			
423	82.8441	no match	0.29	150			

Rank	m/z	Formula	Maximum concentration /ng/m3	Desorption Temp. of max. conc. /°C	Description	Literature	H2O relatives
424	253.178	13CC17H21NH+	0.29	150			
425	219.168	C10H22O3N2H+	0.29	350			
426	287.148	C14H22O6H+	0.28	200			
427	373.088	no match	0.27	150			
428	235.165	C10H22O4N2H+	0.27	150			
429	191.176	C9H22O2N2H+	0.27	100			
430	237.212	no match	0.27	150			
431	41.0866	no match	0.27	150			
432	594.142	no match	0.26	100			
433	268.259	no match	0.26	150			
434	210.193	13CC13H24OH+	0.25	100			
435	245.157	C15H16O3H+	0.25	350			
436	280.16	13CC10H22O6N2H+	0.25	150			
437	108.804	no match	0.23	150			
438	179.175	no match	0.23	350			
439	221.076	C7H12O6N2H+	0.23	250			
440	257.099	C7H16O8N2H+	0.22	150			
441	259.185	no match	0.22	150			
442	242.12	13CC10H16O4N2H+	0.22	200			
443	120.047	13CC2H6O3N2H+	0.2	150			
444	303.273	13CC16H35O3NH+	0.2	150			
445	221.148	C9H2OO4N2H+	0.19	150			
446	286.275	C17H35O2NH+	0.17	150			
447	192.137	C12H17ONH+	0.15	150			
448	358.06	no match	0.14	150			
449	120.039	13CC3H6O4H+	0.13	150			
450	260.186	C13H25O4NH+	0.11	150			
451	581.1	no match	0.1	100			

References

Bayle, K., Gilbert, A., Julien, M., Yamada, K., Silvestre, V., Robins, R. J., Akoka, S., Yoshida, N., and Remaud, G. S.: Conditions to obtain precise and true measurements of the intramolecular 13C distribution in organic molecules by isotopic 13C nuclear magnetic resonance spectrometry, Anal. Chim. Acta., 846, 1–7, doi:10.1016/j.aca.2014.07.018, http://www.sciencedirect.com/science/article/pii/S0003267014008630, 2014.

Camredon, M., Hamilton, J. F., Alam, M. S., Wyche, K. P., Carr, T., White, I. R., Monks, P. S., Rickard, A. R., and Bloss, W. J.: Distribution of gaseous and particulate organic composition during dark alpha-pinene ozonolysis, Atmos. Chem. Phys., 10, 2893–2917, doi:10.5194/acp-10-2893-2010, http://www.atmos-chem-phys.net/10/2893/2010/, 2010.

Cappellin, L., Karl, T., Probst, M., Ismailova, O., Winkler, P. M., Soukoulis, C., Aprea, E., Märk, T. D., Gasperi, F., and Biasioli, F.: On Quantitative Determination of Volatile Organic Compound Concentrations Using Proton Transfer Reaction Time-of-Flight Mass Spectrometry, Environ. Sci. Technol., 46, 2283–2290, doi:10.1021/es203985t, http://pubs.acs.org/doi/abs/10.1021/es203985t, 2012.

Caytan, E., Remaud, G. S., Tenailleau, E., and Akoka, S.: Precise and accurate quantitative 13C NMR with reduced experimental time, Talanta, 71, 1016–1021, doi:10.1016/j.talanta.2006.05.075, 2007b.

Caytan, E., Botosoa, E. P., Silvestre, V., Robins, R. J., Akoka, S., and Remaud, G. S.: Accurate Quantitative 13C NMR Spectroscopy: Repeatability over Time of Site-Specific 13C Isotope Ratio Determination, Anal. Chem., 79, 8266–8269, doi:10.1021/ac070826k, 2007.

Hartz, K. E. H., Rosenørn, T., Ferchak, S. R., Raymond, T. M., Bilde, M., Donahue, N. M., and Pandis, S. N.: Cloud condensation nuclei activation of monoterpene and sesquiterpene secondary organic aerosol, J. Geophys. Res., 110, D14 208, doi:10.1029/2004JD005754, http://www.agu.org/pubs/crossref/2005/2004JD005754.shtml, 2005.

Holzinger, R., Kasper-Giebl, A., Staudinger, M., Schauer, G., and Röckmann, T.: Analysis of the chemical composition of organic aerosol at the Mt. Sonnblick observatory using a novel high mass resolution thermal-desorption proton-transfer-reaction mass-spectrometer (hr-TD-PTR-MS), Atmos. Chem. Phys., 10, 10 111–10 128, doi:10.5194/acp-10-10111-2010, http://www.atmos-chem-phys.net/10/10111/2010/, 2010a, 2010-1, 2010.

Jenkin, M. E.: Modelling the formation and composition of secondary organic aerosol from alpha- and beta-pinene ozonolysis using MCM v3, Atmos. Chem. Phys., 4, 1741–1757, doi:10.5194/acp-4-1741-2004, http://www.atmos-chem-phys.net/4/1741/2004/, 2004.

King, S. M., Rosenoern, T., Shilling, J. E., Chen, Q., and Martin, S. T.: Increased cloud activation potential of secondary organic aerosol for atmospheric mass loadings, Atmos. Chem. Phys., 9, 2959–2971, doi:10.5194/acp-9-2959-2009, 2009.

King, S. M., Butcher, A. C., Rosenørn, T., Coz, E., Lieke, K. I., de Leeuw, G., Nilsson, E. D., and Bilde, M.: Investigating Primary Marine Aerosol Properties: CCN Activity of Sea Salt and Mixed Inorganic–Organic Particles, Environ. Sci. Technol., 46, 10 405–10 412, doi:10.1021/es300574u, http://pubs.acs.org/doi/abs/10.1021/es300574u, 2012.

Kleindienst, T., Smith, D., Li, W., Edney, E., Driscoll, D., Speer, R., and Weathers, W.: Secondary organic aerosol formation from the oxidation of aromatic hydrocarbons in the presence of dry submicron ammonium sulfate aerosol, Atmos. Environ., 33, 3669–3681, doi:10.1016/S1352-2310(99)00121-1, 1999.

Lee, A., Goldstein, A. H., Keywood, M. D., Gao, S., Varutbangkul, V., Bahreini, R., Ng, N. L., Flagan, R. C., and Seinfeld, J. H.: Gas-phase products and secondary aerosol yields from the ozonolysis of ten different terpenes, J. Geophys. Res., 111, D07 302, doi:10.1029/2005JD006437, http://www.agu.org/pubs/crossref/2006/2005JD006437.shtml, 2006.

Martin, G. J., Martin, M. L., and Remaud, G.: SNIF-NMR—Part 3: From Mechanistic Affiliation to Origin Inference, in: Modern Magnetic Resonance, edited by Webb, G. A., pp. 1669–1680, Springer Netherlands, doi:10.1007/1-4020-3910-7_187, 2006a.

Martin, M., Zhang, B., and Martin, G. J.: SNIF-NMR—Part 2: Isotope Ratios as Tracers of Chemical and Biochemical Mechanistic Pathways, in: Modern Magnetic Resonance, edited by Webb, G. A., pp. 1659–1667, Springer Netherlands, doi:10.1007/1-4020-3910-7_186, 2006b.

Shilling, J. E., Chen, Q., King, S. M., Rosenørn, T., Kroll, J. H., Worsnop, D. R., McKinney, K. A., and Martin, S. T.: Particle mass yield in secondary organic aerosol formed by the dark ozonolysis of alpha-pinene, Atmos. Chem. Phys., 8, 2073–2088, doi:10.5194/acp-8-2073-2008, www.atmos-chem-phys.net/8/2073/2008/, 2008.

Silvestre, V., Mboula, V. M., Jouitteau, C., Akoka, S., Robins, R. J., and Remaud, G. S.: Isotopic 13C NMR spectrometry to assess counterfeiting of active pharmaceutical ingredients: Site-specific 13C content of aspirin and paracetamol, J. Pharmaceut. Biomed., 50, 336–341, doi:10.1016/j.jpba.2009.04.030, http://www.sciencedirect.com/science/article/pii/S0731708509002738, 2009.

Singleton, Daniel A. and Thomas, Allen A.: High-Precision Simultaneous Determination of Multiple Small Kinetic Isotope Effects at Natural Abundance, J. Am. Chem. Soc., 117, 9357–9358, doi:10.1021/ja00141a030, http://pubs.acs.org/doi/abs/10.1021/ja00141a030, 1995.

Tani, A., Hayward, S., and Hewitt, C.: Measurement of monoterpenes and related compounds by proton transfer reaction-mass spectrometry (PTR-MS), Int. J. Mass Spectrom., 223–224, 561–578, doi:10.1016/S1387-3806(02)00880-1, http://www.sciencedirect.com/science/article/pii/S1387380602008801, 2003.

Tenailleau, E. and Akoka, S.: Adiabatic 1H decoupling scheme for very accurate intensity measurements in 13C NMR, J. Magn. Reson., 185, 50–58, doi:10.1016/j.jmr.2006.11.007, http://linkinghub.elsevier.com/retrieve/pii/S1090780706003818, 2007.

VanReken, T. M., Ng, N. L., Flagan, R. C., and Seinfeld, J. H.: Cloud condensation nucleus activation properties of biogenic secondary organic aerosol, J. Geophys. Res., 110, D07 206, doi:10.1029/2004JD005465, http://www.agu.org/pubs/crossref/2005/2004JD005465.shtml, 2005.

Zelenyuk, A., Yang, J., Song, C., Zaveri, R. A., and Imre, D.: A New Real-Time Method for Determining Particles' Sphericity and Density: Application to Secondary Organic Aerosol Formed by Ozonolysis of alpha-Pinene, Environ. Sci. Technol., 42, 8033–8038, doi:10.1021/es8013562, http://pubs.acs.org/doi/pdf/10.1021/es8013562, 2008.